ACS APPLIED MATERIALS & INTERFACES

Research Article

www.acsami.org

Design Considerations for Electrode Buffer Layer Materials in Polymer Solar Cells

David Bilby,[†] Bradley Frieberg,[‡] Shobhita Kramadhati,[†] Peter Green,[†,‡,∥] and Jinsang Kim*[,†,‡,∥]

[†]Materials Science and Engineering, [‡]Macromolecular Science and Engineering, and [∥]Chemical Engineering, University of Michigan, Ann Arbor, 48109, United States

Supporting Information

ABSTRACT: Electrode buffer layers in polymer-based photovoltaic devices enable highly efficient devices. In the absence of buffer layers, we show that diode rectification is lost in ITO/P3HT:PCBM/Ag (ITO = indium tin oxide; P3HT = poly(3-hexylthiophene); PCBM = phenyl C_{61}-butyric acid methyl ester) devices due to nonselective charge injection through the percolated phase pathways of a bulk heterojunction active layer. Charge-selective injection, and thus rectification and device function, can be regained by placing thin, polymeric buffer layers that break the direct electrode-active layer contact. Additionally, we show that strong active layer−buffer layer interactions lead to unwanted vertical phase separation and a kinked current−voltage curve. Device function is regained, increasing power conversion efficiency from 3.6% to 7.2%, by placing a noninteracting layer between the buffer and active layer. These results guide the design and selection of future polymeric electrode buffer layers for efficient polymer solar cell devices.

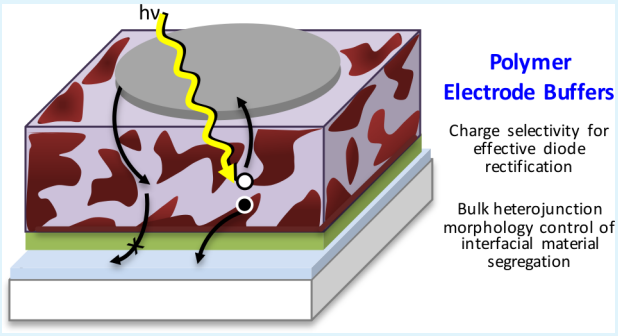

KEYWORDS: *polymer photovoltaic, electrode interface*

INTRODUCTION

Organic photovoltaic (OPV) cells have been a fascinating research topic due to their readily adjustable material and device properties.[1−5] This variability is used in the study of relationships between device structure and performance, with the goal of enabling the practical application of these lightweight materials in roll-to-roll processed, inexpensive, flexible devices.[6−9] The fruits of these efforts have revealed that effective devices typically require fairly complicated structures with multiple layers and controlled mixing of materials; even the nonabsorbing layers within the devices play an important role in power conversion.[10−13]

The structure of OPV devices is critically important for their operation. In short, mixed-material active layers with percolated phase pathways (bulk heterojunction, BHJ, morphologies) are used to overcome exciton binding and diffusion length constraints while not impeding charge extraction.[14−19] The efficiency of OPV devices is also a function of their current-rectifying, diode behavior; if the diode lets its maximum current through under very small positive bias, although it would be a good diode, the photocurrent would be cut off prematurely since it flows opposite to the diode injection. Rectifying character is usually attained or enhanced by placing thin, charge-selective, transparent "buffer" layers between the OPV active layer materials and the electrode contacts.

Electrode buffer materials are used in OPVs to modify the properties of an electrode such that a good electrical contact is formed with the device. Buffer materials are commonly alkali metal compound, oxide, organic, or composite organic-oxide, or metal-oxide based and are deposited with solution or vacuum thermal evaporation methods.[20−25] These materials typically embody many of the characteristics of an ideal electrode and serve to modify or replace the poor characteristics of the outermost electrode. For example, since indium tin oxide (ITO) (work function: 4.5−4.7 eV) often has poor energy level alignment with the transport levels (2.5−4.3 eV lowest unoccupied molecular orbitals (LUMOs), 4.9−6.5 eV highest occupied molecular orbitals (HOMOs)) of the active materials, a buffer that has an appropriate energy level (MoO_3, poly(3,4-ethylenedioxythiophene) polystyrene sulfonate (PEDOT:PSS), etc.) or that modifies the work function of ITO (polyethylenimine (PEIE), self-assembled monolayer, etc.) is chosen.[20,21,26−28] Many effective buffer materials are available, but since their effects on device performance reach beyond energy level alignment, few have been fully characterized.[13,29,30]

Polymeric buffer materials are particularly interesting due to the flexibility afforded to their chemical structure by synthesis. By including charged or polar moieties into their side chains, polymeric buffer materials have been able to either increase or decrease the work function of the electrode onto which they are coated.[24,25,30] These materials have widely varying chemical structures—some have conjugated backbones with thiophene

Received: May 5, 2014
Accepted: August 12, 2014
Published: August 12, 2014

or fluorene, or mixes of monomers, and others are entirely aliphatic. These materials also have varying effects on OPV devices; some polymer buffer materials provide great improvements in device performance, while others do not.[24,30] Finally, some studies identify characteristics of the buffer structure that aid device performance; however, no concrete design principles for effective buffer materials have been outlined.[25,31]

Herein, we study the behavior of OPV devices in the presence or absence of different buffer layers to identify properties of the buffer layers that are beneficial to device operation. We investigate poor OPV device behavior evidenced by shunting or kinked current–voltage curves and present target properties for chemical design that overcome these limitations. The influences of insulating buffer thickness and of the buffer layer–active layer interaction are briefly studied. The design factors that are suggested will counsel the design of future buffer materials that will be applied in high efficiency and flexible OPV devices.

RESULTS AND DISCUSSION

Solar cells fabricated with the structure ITO/PEIE/P3HT:PCBM/MoO_3/Ag (P3HT = poly(3-hexylthiophene); PCBM = phenyl C_{61}-butyric acid methyl ester) provide excellent inverted device behavior. Their diode current under dark conditions (Figure 1) shows suppression of reverse bias leakage and good injection under forward bias. However, if either the anode (MoO_3) or the cathode (PEIE) buffer layer is omitted from the device, the solar cell loses its rectifying behavior. These buffers are crucial not only to operation of the diode, but also to the power conversion process; when a charge-selective buffer layer is left out, high levels of injection under reverse and small forward bias suppress the power conversion efficiency (not shown).

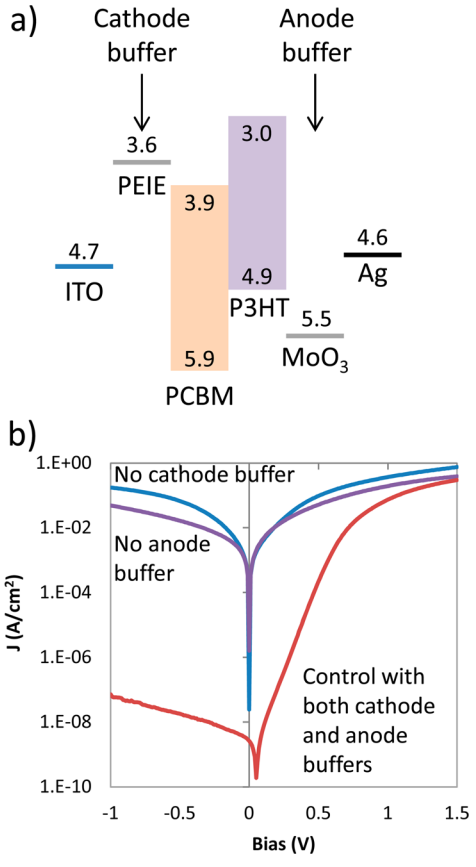

Figure 1. Bulk heterojunction solar cells with the structure ITO/PEIE/P3HT:PCBM/MoO_3/Ag (a) have poor dark diode curves (b) when either buffer layer is omitted. Energy levels are depicted schematically, with disregard for actual interface effects like Fermi level pinning, using literature values.[25,26,32–34,41]

Reverse bias leakage current has few possible origins. Although a chemical reaction between the metal electrode and active materials could plausibly open up a shunting conduction pathway, this explanation cannot account for our loss of rectification when the nonmetallized (ITO side) buffer is omitted.[35] Alternately, electrode penetration through the active materials to make short-type conduction pathways should not be possible since the active layer thickness has not changed. The most likely cause for the loss of current rectification under dark conditions is the nonselective injection of charge carriers into and through the OPV. Since a BHJ morphology allows both materials to have percolated contact between the top and bottom electrodes, nonselective injection into either material can allow charge to flow unobstructed through the device, bypassing the intended diode. A planar heterojunction device, which breaks the interelectrode contact, should not display this character.[36–38]

Inverted, planar heterojunction devices can be fabricated with the structure ITO/PEIE/PCBM/P3HT/MoO_3/Ag by using a contact film transfer process.[5,32] These devices prevent percolative contact of a single material in an OPV with both electrodes, but still display effective diode and photovoltaic characteristics, as shown in Figure 2.

The planar heterojunction device J–V curves begin to take on strange shapes once either of the buffers is removed. When the anode buffer is removed, the dark condition curve displays an increased series resistance, in comparison to the control device, and does not have a low-bias kink. The photocurrent takes on a strange double kinked shape and has an increase in reverse bias photocurrent extraction. When the cathode buffer is removed, the dark condition curve displays an even greater increase in series resistance and under illumination photocurrent can only be extracted under applied bias. These changes in curve shape can be explained when one considers the role of the buffer in energy level alignment and its impact on carrier injection.[39,40] When a buffer layer is removed, if the innate work function of the electrode falls between the transport energy levels of the active layer (i.e., it presents an injection barrier), then the electric field profile within the device, as well as the primary recombination sites, vary from an ideal case, as shown in Figure 3. This results in strange photocurrent behavior as the electric field becomes positive (even for low bias because uninjectable charges pile up), but the photocurrent remains negative (traveling against the field due to its diffusion driven component).[39] The photocurrent eventually gets cut off with increasing bias, but this happens at a potential before injection can effectively "turn on," leading to the curve displaying a kink (no anode buffer) or not displaying a rise of injection at all (no cathode buffer, much higher barrier).

The reverse-bias dark condition curves do not greatly increase in current flow when either buffer layer is removed from the planar heterojunction device. That is to say, in spite of direct contact between an electrode and one of the active materials, and in contrast to BHJ devices, shunting conduction pathways are not introduced.[39] This evidence supports the idea that the buffer prevents percolative contact between the two

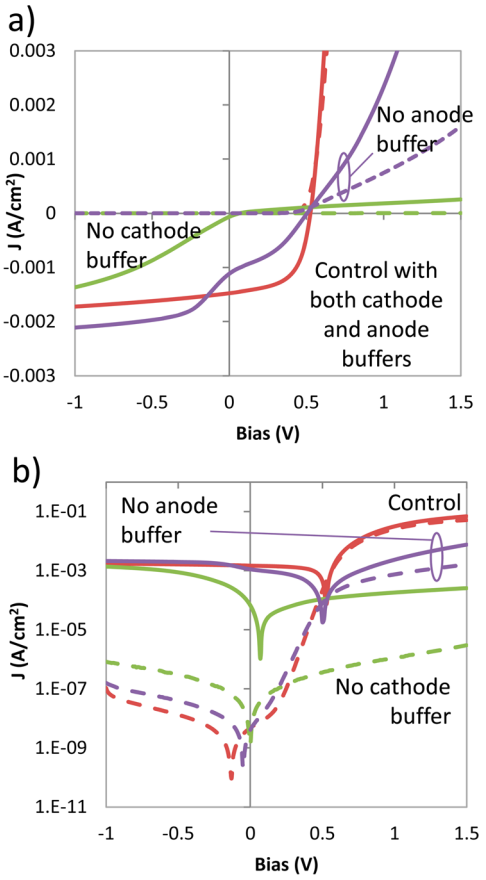

Figure 2. Characteristics of planar heterojunction P3HT/PCBM OPVs (a) under illumination (solid lines) and in the dark (dashed lines) when fabricated with or without cathode or anode buffer layers. The semilog plot, (b), shows the dark condition curves more clearly, indicating retention of rectifying behavior in spite of the absence of buffer layers.

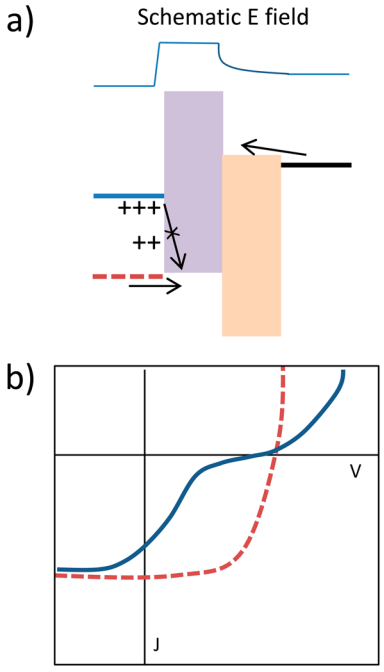

Figure 3. A depiction of good (red) and poor (blue) energy level alignment between the electrode and active layer (a) and its influence on current-bias character (b). Although charge can easily exit the device under reverse bias, poor alignment results in a charge buildup (arrows) as bias is increased, creating a positive internal electric field. The diffusively driven photocurrent flows against the electric field. Photocurrent is reduced as bias is increased, but injection does not turn on until charge can overcome the barrier (to meet and recombine).[39] The result is a kinked $J-V$ curve.

electrodes through one of the BHJ components and thus suppresses leakage current flow.

Direct conduction across one of the materials within a BHJ device is tested by fabricating single material devices using layer thicknesses matching the planar heterojunction devices. Four devices are fabricated; the devices structured ITO/PEIE/P3HT/Ag or ITO/PEIE/PCBM/Ag will test electron injection through the materials while the devices ITO/P3HT/MoO_3/Ag and ITO/PCBM/MoO_3/Ag will test hole injection. As shown in Figure 4, the charge conduction behavior of single material devices differs greatly depending upon the material and upon the presence and type of buffer material. Additionally, these devices do not show strongly rectifying current−voltage character. When P3HT is contacted with a relatively high work function buffer, MoO_3, current can easily pass (likely hole conduction across P3HTs HOMO under positive or negative bias), but when it is contacted with PEIE, which modifies ITO to have a low work function, current is suppressed. Similarly, PCBM gives a fair amount of current when contacted with PEIE (again, likely electron conduction across its LUMO), but it does not give much current flow initially when contacted with MoO_3. Although PCBM does show an increase in current after later scans when contacted with MoO_3 (device burn-in likely aids the contact), this experiment shows that charge-selective electrodes are needed or else charge can be carried across a device at any bias through the percolation pathways of a single material.

The main shunting conduction pathway in BHJ OPVs can be suppressed by using charge-selective electrodes. Although it is well-known that charge selectivity results from appropriate energy level alignment, tests with planar heterojunction devices suggest that a simple interruption of material percolation will produce charge selectivity in OPVs.[39] Recently, research has demonstrated the use of wide band-gap polymeric materials as device-improving buffer layers in organic electronic devices, in line with our hypothesis.[42−44] Devices with the structure ITO/PEIE/P3HT:PCBM/polystyrene (PS)/Ag are fabricated by transferring PS films of different thicknesses (spincast between 750 and 6000 rpm from 2 mg/mL toluene solution) onto BHJ devices using a contact film transfer process.[5,32] Polystyrene is a wide band-gap insulator without any potential to modify the electrode work function or to carry charge. Devices made with PS anode buffer layers show a high series resistance and suppressed reverse-bias dark current, as shown in Figure 5.

It is notable that the dark current in reverse bias does not vary much between the different thicknesses of PS, while the photocurrent varies greatly. The polymeric buffer has suppressed photocurrent extraction, acting as a barrier to charge conduction, but this effect is reduced with the thickness of the PS. Thinner PS allows for more photocurrent to pass and a slight recovery of the normal $J-V$ character of an OPV. However, the injection and extraction barriers presented by the PS and the poor energy alignment of the Ag electrode with the active layer prevent an easy onset of injection and prematurely cut off extraction, leading to a kinked curve with a low fill factor

dx.doi.org/10.1021/am502673e | ACS Appl. Mater. Interfaces 2014, 6, 14964−14974

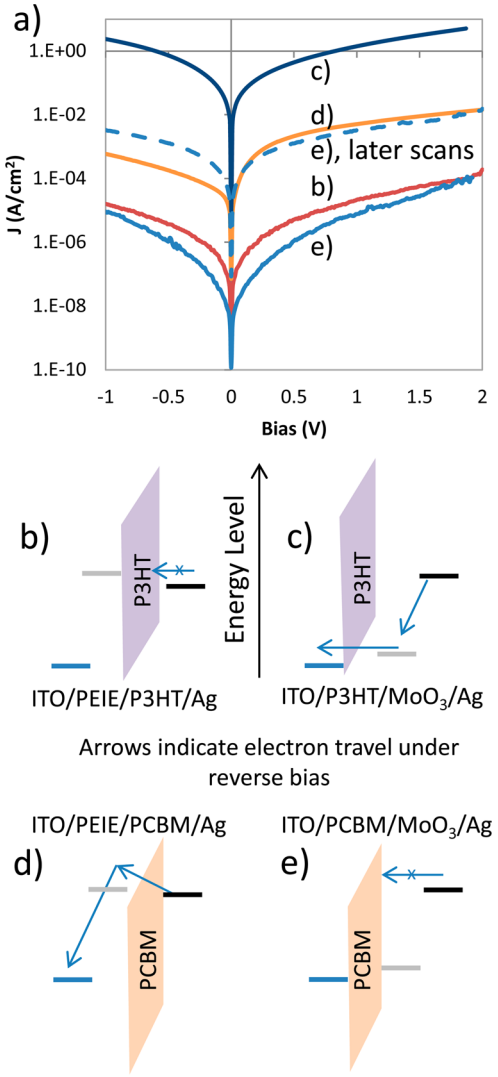

Figure 4. Current–voltage characteristics of single materials devices measured in the dark, (a), schematically depicted to the right under reverse bias, (b–e), with literature values for energy levels.[25,26,32,33,40,41] Energy level alignment between the electrode and active layer moderates charge carrier injection and current magnitude.

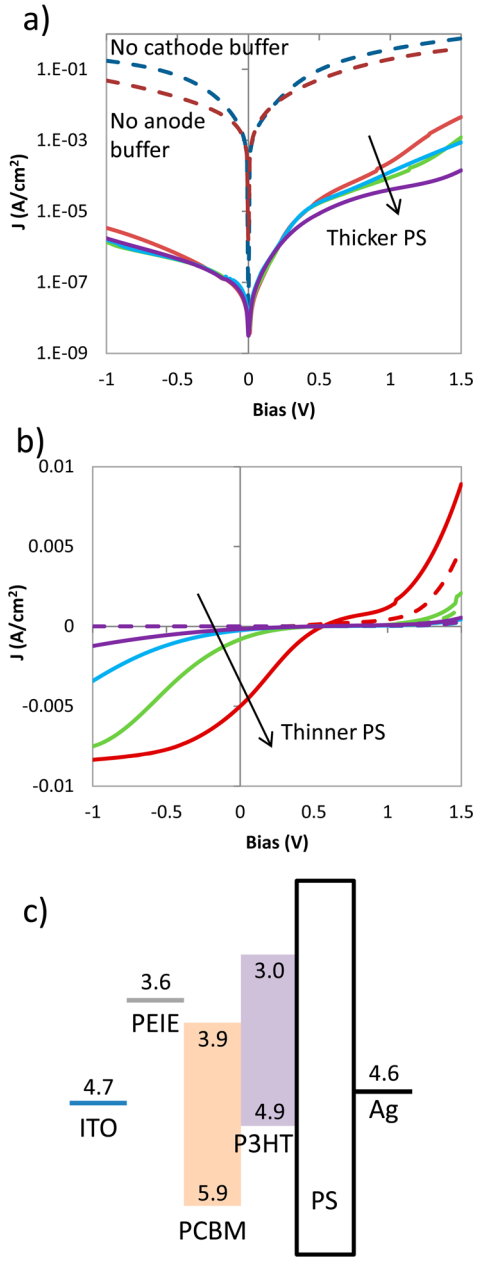

Figure 5. Characteristics of ITO/PEIE/P3HT:PCBM/PS/Ag devices in the dark (a) and under illumination (b). The thickness of the PS is controlled through spincasting speed variation between 750 and 6000 rpm. The energy levels of PS, (c), estimated based on a band gap greater than 4 eV, should retard charge injection into the device.[25,26,32,41,45]

(FF). In all thicknesses probed, the polymeric buffer layer suppresses the reverse bias leakage by acting as a barrier to the injection or extraction of the incorrect charge (electrons) at the anode.

It is plausible to suggest that the inclusion of a polymer buffer leads to the recovery of photovoltaic behavior by simply acting as a resistor that suppresses injection or extraction of charge carriers. Under illumination, this reduced extraction at the anode, in combination with the electron-selective cathode, leads to an increased electron diffusion current away from the anode, and the seeming recovery of photovoltaic operation.[39] Since this mechanism would require tunneling transport of holes through the polymer anode, devices with thinner anode buffer layers are fabricated. Devices with the structure ITO/PEIE/P3HT:PCBM/PPECN/Ag are fabricated by transferring monolayer films of poly(2-cyanohexyloxy-5-decyloxyphenylene-1,4-ethynylene) (PPECN) onto the active materials. Monolayers of PPECN are spread at the air–water interface and compressed to 25 mN/m, and films are transferred using Langmuir–Schaefer (LS) lifting or Langmuir–Blodgett (LB) transfer. By lifting multiple monolayers, the thickness of the buffer can be controlled with finesse. Although PPECN has a conjugated backbone, its conductivity is very poor, and its HOMO level (~5.6 eV) is too deep to easily inject charge onto P3HT (4.9 eV). Finally, PPECN does not appear to affect electrode work function, so it is treated as an insulating buffer material.

Photovoltaic devices fabricated with very thin PPECN insulating buffer layers show a decrease in reverse bias leakage current and an increase in series resistance, similar to PS, as shown in Figure 6. The dependence of the OPV characteristics upon anode buffer layer thickness shows multiple trends. First, the choice of technique (LS or LB) used to increasing the

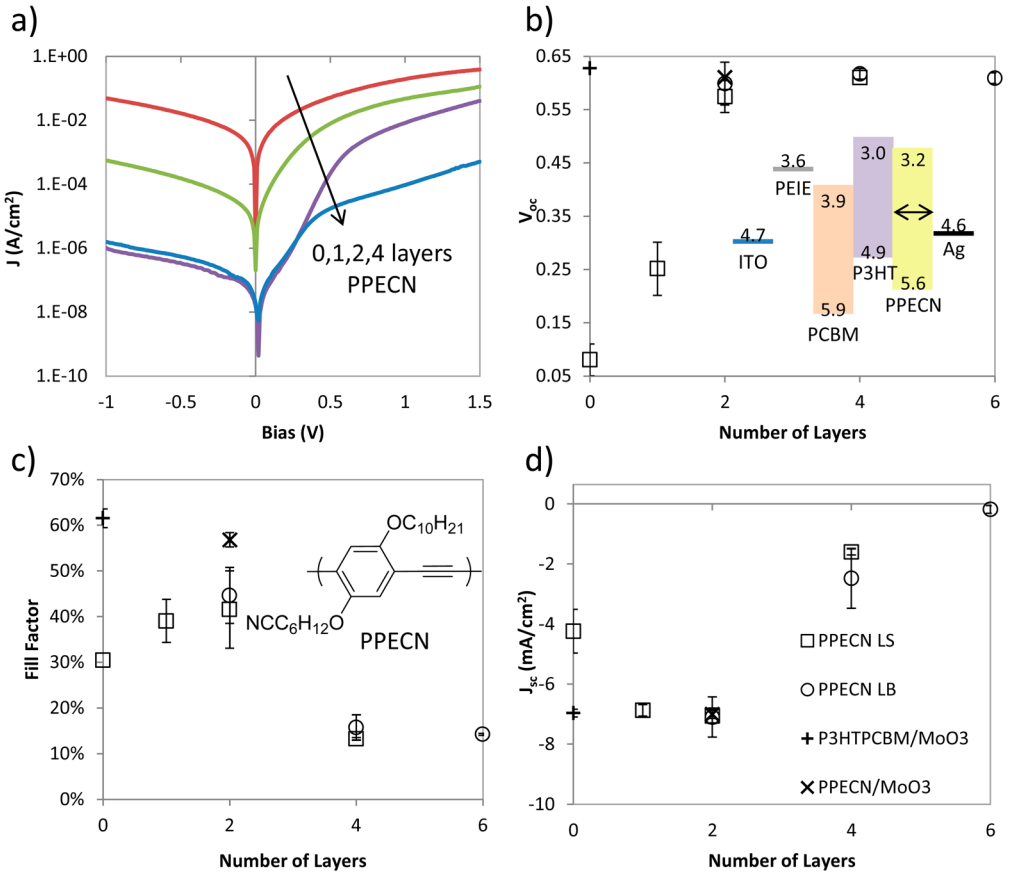

Figure 6. Photovoltaic behavior of ITO/PEIE/P3HT:PCBM/PPECN/Ag OPVs with multilayer PPECN anode buffer layers. Dark condition current–voltage characteristics (a) dramatically change as up to six PPECN layers are added via Langmuir–Schaefer (LS) lifting or Langmuir–Blodgett (LB) transfer. Photocurrent behavior including V_{oc} (b), fill factor (c), and J_{sc} (d) also change. Control devices have MoO_3 or PPECN/MoO_3 anode buffer layers. The energy levels of PPECN act as a blocking layer relative to those of the active layer and electrodes, with literature values for energy levels, as depicted in the inset of (b).[25,26,32,34,41]

thickness of the PPECN layer does not appear to influence the device behavior. As the PPECN thickness is increased to two layers, the reverse bias leakage current drops and saturates (Figure 6a). There is also a recovery of short circuit current density (J_{sc}), open circuit voltage (V_{oc}), and a partial recovery of FF. At the same time, the series resistance continues to rise over the addition of six layers of PPECN and there is a drop in FF and J_{sc}; the increase in series resistance is likely the cause for the drop in J_{sc} and FF at higher buffer thicknesses. Also, just as with PS, the PPECN buffer is not work function modifying and acts as an extraction barrier, so the poor electrode and buffer energy level alignment with the active materials leads to a premature decrease in photocurrent, (hence a kinked J–V curve (not shown) and a reduced FF), even at optimal buffer thickness.

The initial recovery of the diode rectification, V_{oc}, and J_{sc} is interesting; a simple resistor that is not charge-selective would suppress photocurrent extraction as well as reverse and forward bias injection. This diode rectification recovery suggests that the PPECN buffer is imparting charge selectivity. Since the cathode is electron selective, it extracts electrons from the device and leaves the holes, with nowhere else to go, to tunnel through the PPECN buffer. Thus, when the PPECN layer is very thin, it allows the hole current to tunnel through while still suppressing the shunting, reverse bias and low forward bias injection/extraction processes. This leads to a recovery of J_{sc} (diffusion-driven photocurrent is extracted once nonselective extraction is suppressed) and V_{oc} (since charges are no longer extracted at the wrong electrode, and low forward bias dark current is suppressed). The fact that the reverse and low forward bias dark current decreases by 5 orders of magnitude, while the injection (higher positive bias dark) current only drops by about 1 order of magnitude is also evidence for the recovery of charge selectivity at the anode.

Designing devices with charge-selective electrodes does not guarantee excellent performance with all active layer materials. Inverted OPV devices with the structure ITO/PEIE/P3HT:PCBM/MoO_3/Ag have exemplary device characteristics. The PEIE and MoO_3 buffer layers prevent contact between the electrode and active layers and they modify the electrode work function, providing excellent charge selectivity and easy charge injection and extraction.[25] However, when the same buffer layers are applied to poly[[9-(1-octylnonyl)-9*H*-carbazole-2.7-diyl]-2.5-thiophenediyl-2.1.3-benzothiadiazole-4.7-diyl-2.5-thiophenediyl (PCDTBT) devices, as shown in Figure 7, the photovoltaic character is damaged, and a kink appears in the current–voltage curve.

Even in the presence of charge-selective electrodes, improper device morphology can critically limit photovoltaic performance. For instance, if the components of the BHJ are poorly miscible due to a mismatch in surface energy, then massive phase segregation can prevent easy exciton dissociation and charge extraction, potentially resulting in a kinked J–V curve. Water contact angle is considered as a pseudocharacterization

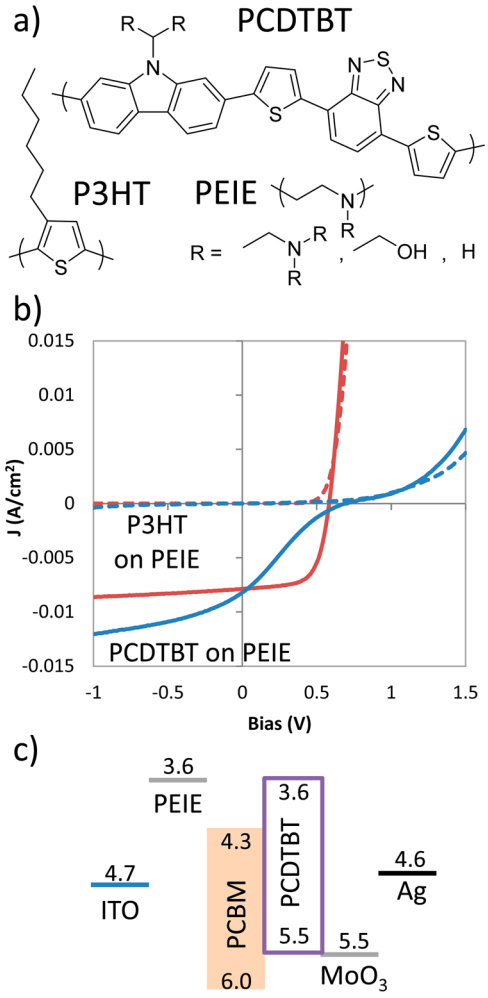

Figure 7. Chemical structure of PCDTBT, P3HT, and PEIE (a) and the OPV characteristics of inverted P3HT and PCDTBT devices where PEIE is the cathode buffer layer (b). The energy levels of the PCDTBT device, (c), are drawn from literature values.[23,25,26,33,41] The P3HT device diagram can be seen in Figure 1.

of surface energy and, as shown in Table 1, the values for P3HT, PCDTBT, and the two PCBMs are compared.

Table 1. Water Contact Angles of P3HT, PCDTBT, PCBM, PC70BM, and PEIE

	P3HT	PCDTBT	PCBM	PC70BM[a]	PEIE
water contact angle (deg)	90 ± 4	92 ± 2	63 ± 2	65 ± 1	9 ± 1

[a]Phenyl C_{71}-butyric acid methyl ester.

The water contact angles of the conjugated polymers in Table 1 are very similar to each other (as are the fullerenes). Although the makeup of the active layer of each device contains a different mass fraction of fullerene, the similarity between the constituent material water contact angles suggests that there is not some massive chemical incompatibility within the active layer, which is causing device limiting phase separation. Indeed, many others have optimized devices and morphologies with the same active layer materials and blending ratios that are used here.[46] The difference between P3HT and PCDTBT inverted device characteristics is likely due to the buffer layer–active layer interface.

The impact of morphology on device behavior can be ruled out by making planar heterojunction devices. In this case, by making planar heterojunction PCDTBT devices (ITO/PEIE/PCBM/(PCDTBT or P3HT)/MoO_3/Ag) the interface with the PEIE buffer is forced to be entirely PCBM. Thus, the planar device is expected to show which component of the BHJ at the buffer interface is responsible for the poor device behavior. As shown in Figure 8, PCDTBT and P3HT planar heterojunction devices on PEIE both have nonkinked current–voltage characteristics.

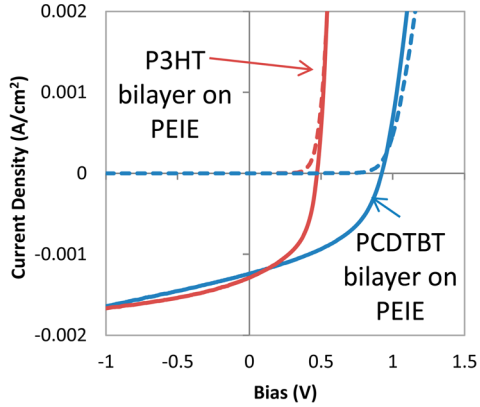

Figure 8. Current–voltage characteristics of planar heterojunction PCDTBT and P3HT devices with PEIE cathode buffer layers do not exhibit kinked curves.

The planar heterojunction ITO/PEIE/PCBM/PCDTBT/MoO_3/Ag devices show that the PEIE/PCBM interface is not responsible for kinked *J*–*V* curves. This is not surprising since the P3HT planar and BHJ devices each have this same interface and since they function well. Instead, it appears that the interface between PCDTBT and PEIE is responsible for the kink in the device curve. Further, since BHJ OPVs with other conjugated polymers, such as P3HT, do not show this character, and since it is known that extraction barriers lead to kinked device curves, we hypothesize that there is some interaction that preferentially pulls PCDTBT to the cathode buffer interface.[39,40] This vertical segregation of polymer acts as a charge-extraction and charge-injection barrier for electrons on PCBM, as shown in Figure 9.

Variable angle spectroscopic ellipsometry was used to check our suspicion; by fitting ellipsometric data from a film of glass/PEIE/PCDTBT:PC70BM using previously measured optical constants for glass, PEIE, PCDTBT, and PC70BM, we are able to see the surface segregation (shown in the Supporting Information). A Cauchy model is used, along with an effective medium approximation, to fit the thickness and PCBM concentration of the film. Then, the film is modeled as two consecutive PCDTBT:PC70BM layers on glass/PEIE. This fitting method is used to approximate the thickness, if any, of a surface segregated PCDTBT layer. The PCDTBT:PC70BM film is found to be about 56 nm thick, with a PC70BM concentration of 82%, which is appropriate for the 1:4 mixing ratio. Further, fitting the thickness of a PCDTBT region of the film with 0% PC70BM near the PEIE layer gives 1.38 nm. Although this method may not quantitatively prove pure interface separation of PCDTBT, it does support our hypothesis that the interface is PCDTBT-rich. The evidence that PCDTBT is segregated to the PEIE interface is suggestive

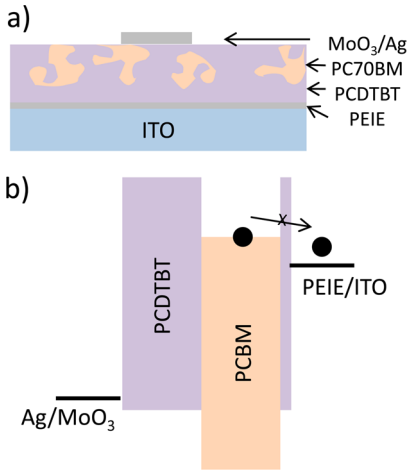

Figure 9. Depictions of the ITO/PEIE/PC70BM:PCDTBT/MoO_3/Ag device structure (a) and energy level diagram (b) when PEIE is used as a cathode buffer. PCDTBT has an interaction with PEIE that segregates PCDTBT to the cathode creating an electron (●) collection and injection barrier.

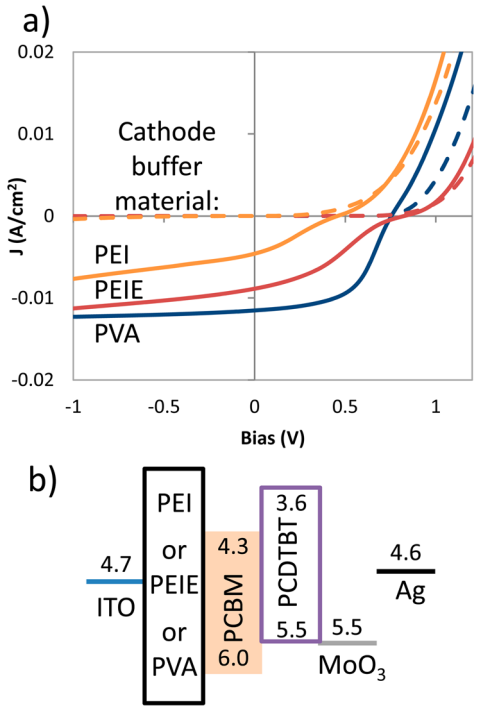

Figure 10. Kink in the OPV current–voltage sweep changes (a) with changing cathode buffer in ITO/cathode buffer/PCDTBT:PC70BM/MoO_3/Ag devices. This suggests reduced PCDTBT/buffer interaction as the amount of amine functionality in the buffer is reduced. The device schematic, (b), is depicted with energy levels from other papers.[23,25,26,33,41]

of a chemical interaction between the two materials. During spincasting, as the PCDTBT:PCBM film dries on top of the buffer, the interaction between PCDTBT and the buffer drives the formation of the morphology of the film. The absence of this interaction between P3HT and PEIE can explain why P3HT-based devices do not exhibit this depreciatory behavior. This model is consistent with previous research wherein P3HT is shown to vertically segregate based upon surface energy interactions, independent of the presence of PEIE.[47,48] However, this result is not consistent with the work of Sach-Quintana et al., who reported a similar PCDTBT device architecture (albeit with water washed PEIE) and made no mention of kinked J–V curves.[47]

Since this interaction manifests as vertical phase separation, which is detrimental to OPV function, changing the chemical character of the cathode buffer layer should lead to a change in device operation. For instance, by reducing the amount of amine functionality within the buffer by switching from poly(ethylenimine) (PEI, all amine), to poly(ethylenimine, ethoxylated) (PEIE, some of the amines have been ethoxylated and are hydroxyl-terminated) to 80% hydrolyzed poly(vinyl alcohol) (PVA, no amine, mostly hydroxyl) the influence of buffer chemical structure on the PCDTBT OPV device operation can be monitored. This change alludes to changes in the active layer–buffer interaction. As shown in Figure 10 and Table 2, changing the cathode buffer from PEI to PEIE or to PVA drastically changes device performance.

As the amount of amine functionality in the cathode buffer is reduced, the kink in the J–V curve of PCDTBT devices is reduced, and the FF, J_{sc}, and power conversion efficiency (PCE) all increase. Although the thickness of these insulating buffer layers is not explicitly controlled (optimization presented in the Supporting Information), the concentration (0.4 wt %) and spincasting rates (3000 rpm) for PEIE and PEI are held the same, and PVA (2 mg/mL) is also similar. Since the series resistances (qualitatively shown in Supporting Information) of these devices are also all very similar, we expect that buffer thickness is not limiting the performance of these devices. Rather, the differences between these devices likely stems from differences in buffer–PCDTBT interaction strength that leads to differences in vertical segregation of the active layer materials.

Table 2. Photovoltaic Properties of PCDTBT Devices with Different Cathode Buffer Layers

cathode buffer	PEI	PEIE	PVA
V_{oc}	0.43 ± 0.02	0.79 ± 0.06	0.72 ± 0.02
J_{sc} (mA/cm^2)	4.3 ± 0.3	8.7 ± 0.2	11.2 ± 0.1
FF (%)	27 ± 1	32 ± 1	54 ± 1
PCE (%)	0.51 ± 0.06	2.2 ± 0.1	4.3 ± 0.3

It appears that amine functionality has an interaction with PCDTBT. To characterize the interaction strength between buffers with particular functionality and PCDTBT, dissolution studies are performed. PCDTBT is spincast upon different buffer materials, and the whole film is immersed in 1,2-dichlorobenzene (a good solvent for PCDTBT) for 10 min. If there is a strong buffer–PCDTBT interaction, some PCDTBT will not dissolve. The change in peak PCDTBT absorption (575 nm) strength after the solvent soak, as shown in Table 3, is used as a pseudomeasurement of interaction strength.

The dissolution studies corroborate the OPV device characteristics in light of the hypothesis of interaction-driven interface segregation. There is an increase in remaining PCDTBT absorption as the hydrophilicity (from poly-(vinylacetate), PVAc, to 100% hydrolyzed PVA) and amount of amine functionality (from PVA to PEI) increase. This trend mirrors the device characteristics, and suggests that control over the interaction strength, through control over chemical structure of the buffer layer, leads to control over the level of interface segregation of PCDTBT in BHJ OPVs. This control can ultimately lead to influence over the shape of the J–V

Table 3. Dissolution Studies Provide an Indication of Buffer−PCDTBT Interaction Strength

buffer[a]	remaining absorption[b] of PCDTBT (%) at 575 nm
PEO	66 ± 9[c]
PEI	61 ± 5
glass	58 ± 5
PEIE	40 ± 8
PEDOT:PSS	36 ± 4
PVA100	33 ± 6
PVA80	24 ± 1
PVAc	15 ± 4[c]

[a]Stronger interactions lead to less dissolution and greater remaining absorption strength. [b]Error bars are from 2 to 4 samples for each condition. [c]PEO and PVAc have some solubility in 1,2-dichlorobenzene, but this does not seem to dictate the measured dissolution.

curve, as has been previously shown for P3HT devices; in conventional architecture P3HT:PCBM devices, kinked $J-V$ curve shapes that are caused by free-surface (cathode) segregation of P3HT can be repaired by placing a thin fullerene layer at the cathode interface.[49]

Photovoltaic devices are fabricated with compound cathode buffer layers to tune the strength of the buffer−PCDTBT interaction. As shown in Figure 11 and Table 4, PCDTBT

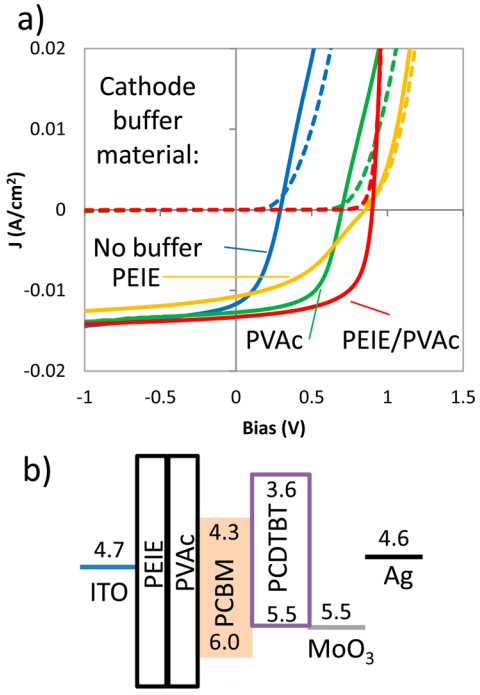

Figure 11. PCDTBT devices with different cathode buffer layers. When a noninteracting buffer material, like PVAc, is placed between two interacting layers, PCDTBT and PEIE, the influence of the interaction of device character, (a), is suppressed. The device schematic, (b), is depicted with energy levels from other papers.[23,25,26,33,41]

OPVs with PVAc cathode buffer layers do not show kinked $J-V$ curves. PVAc is spincast at 3000 rpm from 1 mg/mL solution in dimethylformamide (DMF) and, in spite of its dilution, makes a noticeable difference on device performance in comparison to a device with no cathode buffer. The work function of the compound buffer layer is compared to its constituent materials through kelvin probe measurements relative to ITO. As shown in the Supporting Information, the work function shift caused by the compound buffer layer is similar to that of PEIE, in spite of the insulating, nonwork function modifying PVAc layer on top. The work function shift measured for PEIE is similar to literature values.[25]

The inclusion of a cathode buffer layer that does not have a strong interaction with PCDTBT does not lead to unfavorable vertical phase separation in OPV devices. By placing the polymeric cathode buffer, PVAc, into PCDTBT devices, the V_{oc} and J_{sc} increase, relative to a device with no cathode buffer layer, as the onset of injection current is suppressed (see semilog plots in Supporting Information). More so, since PVAc does not pull PCDTBT to the cathode interface, charge extraction is not reduced and the J_{sc} is greater than devices with PEIE cathode buffer layers. However, since PVAc does not reduce the work function of ITO the V_{oc} is limited by the injection barrier at the cathode contact with the BHJ morphology active layer (recombination of holes at the electron collecting electrode).[39] Previous devices with PEIE do not show a severely limited V_{oc}; however, the interaction strength with PCDTBT is device-limiting. Thus, we fabricate devices with a compound buffer layer where PVAc is spincast on top of the PEIE, acting as a morphology directing layer that tempers the interface with PCDTBT. The compound cathode buffer layer devices show excellent behavior, displaying all of the positive characteristics of each buffer; a high V_{oc}, J_{sc}, FF, and PCE of 7.2% result when the cathode buffer-active layer interaction strength is appropriately controlled and its work function is appropriate for good electrical contact.

CONCLUSION

The design of new buffer layer materials for high-performance OPVs requires that the loss routes in the device that the buffer improves are known and that the role of the buffer in mitigating this loss is understood in terms of the chemical structure of the buffer. We have shown that shunting conduction pathways, caused by nonselective charge injection and conduction across one of the components of the active material of a BHJ OPV, leads to loss of diode rectification and photovoltaic power conversion behavior. This shunting loss route is avoided by imparting charge selectivity to the electrodes. Further, nonselective Ag anodes are improved by placing a thin, polymeric buffer layer between the electrode and active layer. The incorporation of the buffer layer seemingly provides charge selectivity to the dark (diode) current and suppresses extraction of charge, which in combination with the highly selective opposite electrode, provides a partial recovery of photovoltaic performance. The design of effective buffer materials for high-efficiency OPVs also requires knowledge of the role of the buffer in device morphology development. We have shown that a strong interaction between a cathode buffer material (PEIE) and the hole conducting conjugated polymer (PCDTBT) in the active layer of a BHJ OPV leads to device-harming segregation of the polymer to the buffer interface. This interaction appears to originate from interaction with the hydrophilic, amine functionality of PEIE, and manifests in devices as kinked current−voltage behavior due to the interfacial electron injection/extraction barrier that the polymer becomes. By placing noninteracting materials between PEIE and PCDTBT, the negative device character is repaired resulting in a high PCE. These results provide design rules that justify the use of thin, polymeric buffer materials with

Table 4. Device Properties of PCDTBT OPVs with Different Cathode Buffer Layers

	no cathode buffer	PVAc	PEIE	PEIE/PVAc
V_{oc}	0.28 ± 0.05	0.64 ± 0.09	0.83 ± 0.02	0.88 ± 0.02
J_{sc} (mA/cm^2)	−11.4 ± 0.7	−12.5 ± 0.3	−11.0 ± 0.8	−13.1 ± 0.4
FF (%)	42 ± 2	58 ± 3	40 ± 1	62.7 ± 0.7
PCE (%)	1.4 ± 0.4	4.6 ± 1	3.6 ± 0.3	7.2 ± 0.2

tempered active layer interaction and will help enable the design of electrode buffer layers for high efficiency OPVs.

EXPERIMENTAL PROCEDURES

All materials are used as purchased. Poly(3-hexylthiophene) (P3HT), P100 or RMI-001EE, is purchased from Rieke Metals, poly[*N*-9′-heptadecanyl-2,7-carbazole-*alt*-5,5-(4′,7′-di-2-thienyl-2′,1′,3′-benzothiadiazole)] (PCDTBT), SOL4280, is purchased from Solaris Chem Inc. Phenyl C_{61}-butyric acid methyl ester (PCBM), ADS61BFA, is purchased from American Dye Source, and phenyl C_{71}-butyric acid methyl ester (PC70BM), 910−1500, is purchased from SES Research. ITO-coated glass, CG-50IN-S107, is purchased from Delta technologies, Ltd., All of the polymer buffer materials are purchased from Sigma-Aldrich, as are MoO_3 and the constituent materials for the poly(phenylene ethynylene) (PPECN) buffer, as depicted the Supporting Information. Silver pellets are purchased from Kurt J. Lesker.

Multilayer films of the PPECN buffer material are deposited from monolayers spread at the air−water interface from a 5.9 mg/mL solution in chloroform. The monolayers are compressed to 25 mN/m with a NIMA Langmuir−Blodgett trough for transfer.

Bulk heterojunction polymer solar cells, with a structure of ITO/buffer 1/PCBM:polymer/buffer 2/Ag are fabricated by spincasting, film transfer, and vacuum thermal evaporation. ITO glass is sonicated in isopropanol and then acetone, in each case for 10 min, followed by a 10 min UV−ozone treatment. Next, buffer 1 is spincast in a nitrogen-filled glovebox. ITO covering buffers are commonly cast (2 mg of PVA/mL of DMF, 1 mg of PVAc/mL of DMF, 2 mg PEO/mL MeOH) at 3000 rpm/30 s and annealed at 100 °C/10 min, excepting PEIE and PEI, which are cast from a 0.4 wt % in 2-methoxyethanol solution at 3000 rpm for 1 min, accelerating at 1000 rpm/s.[25] The active layer is then spincast and annealed (either P3HT:PCBM, 1:1 by weight, 10 mg polymer/mL chlorobenzene, 1000 rpm/30 s, 150 °C/15 min or PCDTBT:PC70BM, 1:4 by weight, 1.75 wt % in 1:3 chlorobenzene/1,2-dichlorobenzene by volume, 1500 rpm/30 s, 70 °C/15 min).[46] In some devices, buffer 2 is deposited via film transfer of PPECN monolayers (as above) or of polystyrene from (2 mg/mL in toluene) sacrificial poly(sodium styrenesulfonate) substrates. Finally, the top electrode is deposited at pressures below 5×10^{-7} Torr; after buffer 2 (commonly 10 nm of MoO_3), Ag (100 nm) is deposited through a circular shadow mask of 1 mm in diameter.

Bilayer devices, ITO/PEIE/PCBM/polymer/MoO_3/Ag, are fabricated in a manner similar to previous routes, where the polymer layer is transferred from a sacrificial substrate onto PCBM (for P3HT) or PC70BM (for PCDTBT).[5,32] PCDTBT is cast from 10 mg/mL *o*-dichlorobenzene, at 6000 rpm/30 s, and both types of PCBM films are cast from 30 mg/mL chlorobenzene at 1000 rpm/60 s followed by a 150 °C/15 min anneal. These active-layer casting conditions are also used for single-active material devices.

Photovoltaic devices are characterized with an HP/Agilent semiconductor parameter analyzer while being illuminated with simulated AM 1.5G, 1 sun light from a Newport solar simulator. The device current is normalized to the electrode mask size. Typically, nine devices on one substrate are made for each condition, and *J*−*V* curves, which clearly show leaky or short-like behavior, are dropped. Devices that are fabricated during the same day are typically compared, since there is a large day-to-day variation in devices with kinked *J*−*V* curves.

Absorption of the polymer films is measured using transmission mode in a Varian Cary 50 spectrometer. The quality of the monolayer films is observed macroscopically with an Olympus BX-51 fluorescence/optical microscope.

Work function shifts are measured using a homemade kelvin probe with an ITO reference electrode (see Supporting Information).

Cyclic voltammetry is measured with a CH instruments CHI600C potentiostat using 0.1 M tetrabutylammonium hexafluorophosphate in acetonitrile as the working electrolyte, silver nitrate as the reference electrode, and Pt wire as the counter electrode. The scans are taken at the rate of 0.1 V/s and are shifted using the onset of ferrocene oxidation (−4.80 eV). The working electrode is glassy carbon, and HOMO and LUMO values are calculated using the onset of reduction or oxidation.

ASSOCIATED CONTENT

Supporting Information

Synthetic information for PPECN, optimization of the buffer layer thicknesses, semilog *J*−*V* curves for buffer−active layer interaction, a homemade kelvin probe schematic, and work function measurements. This material is available free of charge via the Internet at http://pubs.acs.org.

AUTHOR INFORMATION

Corresponding Author

*E-mail: jinsang@umich.edu.

Notes

The authors declare no competing financial interest.

ACKNOWLEDGMENTS

This work was supported as part of the Center for Solar and Thermal Energy Conversion, an Energy Frontier Research Center funded by the U.S. Department of Energy, Office of Science, Basic Energy Sciences under Award No. DE-SC-0000957.

REFERENCES

(1) Li, G.; Zhu, R.; Yang, Y. Polymer Solar Cells. *Nat. Photonics* **2012**, *6*, 153−161.

(2) Qian, D.; Ma, W.; Li, Z.; Guo, X.; Zhang, S.; Ye, L.; Ade, H.; Tan, Z.; Hou, J. Molecular Design Toward Efficient Polymer Solar Cells with High Polymer Content. *J. Am. Chem. Soc.* **2013**, *135*, 8464−8467.

(3) Henson, Z.; Mullen, K.; Bazan, G. Design Strategies for Organic Semiconductors Beyond the Molecular Formula. *Nat. Chem.* **2012**, *4*, 699−704.

(4) Zhou, H.; Yang, L.; You, W. Rational Design of High Performance Conjugated Polymers for Organic Solar Cells. *Macromolecules* **2012**, *45*, 607−632.

(5) Tada, A.; Geng, Y.; Wei, Q.; Hashimoto, K.; Tajima, K. Tailoring Organic Heterojunction Interfaces in Bilayer Polymer Photovoltaic Devices. *Nat. Mater.* **2011**, *10*, 450−455.

(6) Krebs, F.; Fyenbo, J.; Jørgensen, M. Product Integration of Compact Roll-to-roll Processed Polymer Solar Cell Modules: Methods and Manufacture Using Flexographic Printing, Slot-die Coating and Rotary Screen Printing. *J. Mater. Chem.* **2010**, *20*, 8994−9001.

(7) Bundgaard, E.; Hagemann, O.; Manceau, M.; Jorgensen, M.; Krebs, F. Low Band Gap Polymers for Roll-to-roll Coated Polymer Solar Cells. *Macromolecules* **2010**, *43*, 8115−8120.

(8) Park, H. J.; Kang, M.-G.; Ahn, S. H.; Guo, L. J. A Facile Route to Polymer Solar Cells with Optimum Morphology Readily Applicable to a Roll-to-roll Process without Sacrificing High Device Performance. *Adv. Mater.* **2010**, *22*, E247−E253.

(9) Kim, M.; Kim, J.; Cho, J.; Shtein, M.; Guo, L.; Kim, J. Flexible Conjugated Polymer Photovoltaic Cells with Controlled Heterojunctions fabricated using Nanoimprint Lithography. *Appl. Phys. Lett.* **2007**, *90*, 123113.
(10) He, Z.; Zhong, C.; Su, S.; Xu, M.; Wu, H.; Cao, Y. Enhanced Power-Conversion Efficiency in Polymer Solar Cells using an Inverted Device Structure. *Nat. Photonics* **2012**, *6*, 591−595.
(11) Kim, J.; Kim, S.; Lee, H.; Lee, K.; Ma, W.; Gong, X.; Heeger, A. New Architecture for High-Efficiency Polymer Photovoltaic Cells Using Solution-Based Titanium Oxide as an Optical Spacer. *Adv. Mater.* **2006**, *18*, 572−576.
(12) Hadipour, A.; Cheyns, D.; Heremans, P.; Rand, B. Electrode Considerations for the Optical Enhancement of Organic Bulk Heterojunction Solar Cells. *Adv. Energy Mater.* **2011**, *1*, 930−935.
(13) Guo, X.; Zhou, N.; Lou, S.; Smith, J.; Tice, D.; Hennek, J.; Ortiz, R.; Navarrete, J.; Li, S.; Strzalka, J.; Chen, L.; Chang, R.; Facchetti, A.; Marks, T. Polymer Solar Cells with Enhanced Fill Factors. *Nat. Photonics* **2013**, *7*, 825−833.
(14) Tang, C. Two-Layer Organic Photovoltaic Cell. *Appl. Phys. Lett.* **1986**, *48*, 183−185.
(15) Lee, J.; Vandewal, K.; Yost, S.; Bahlke, M.; Goris, L.; Baldo, M.; Manca, J.; Voorhis, T. Charge Transfer State Versus Hot Exciton Dissociation in Polymer-Fullerene Blended Solar Cells. *J. Am. Chem. Soc.* **2010**, *132*, 11878−11880.
(16) Yu, G.; Gao, J.; Hummelen, J. C.; Wudl, F.; Heeger, A. J. Polymer Photovoltaic Cells: Enhanced Efficiencies via a Network of Internal Donor-Acceptor Heterojunctions. *Science* **1995**, *270*, 1789−1791.
(17) Vithanage, D.; Devizis, A.; Abramavicius, V.; Infahsaeng, Y.; Abramavicius, D.; MacKenzie, R. C. I.; Keivanidis, P.; Yartsev, A.; Hertel, D.; Nelson, J.; Sundstrom, V.; Gulbinas, V. Visualizing Charge Separation in Bulk Heterojunction Organic Solar Cells. *Nat. Commun.* **2013**, *4*, 2334.
(18) Shaw, P. E.; Ruseckas, A.; Samuel, I. D. W. Exciton Diffusion Measurements in Poly(3-hexylthiophene). *Adv. Mater.* **2008**, *20*, 3516−3520.
(19) Lunt, R.; Giebink, N.; Belak, A.; Benziger, J.; Forrest, S. Exciton Diffusion Lengths of Organic Semiconductor Thin Films Measured by Spectrally Resolved Photoluminescence Quenching. *J. Appl. Phys.* **2009**, *105*, 053711.
(20) Ratcliff, E.; Zacher, B.; Armstrong, N. Selective Interlayers and Contacts in Organic Photovoltaic Cells. *J. Phys. Chem. Lett.* **2011**, *2*, 1337−1350.
(21) Po, R.; Carbonera, C.; Bernardi, A.; Camaioni, N. The Role of Buffer Layers in Polymer Solar Cells. *Energy Environ. Sci.* **2011**, *4*, 285−310.
(22) Shrotriya, V.; Li, G.; Yao, Y.; Chu, C.; Yang, Y. Transition Metal Oxides as the Buffer Layer for Polymer Photovoltaic Cells. *Appl. Phys. Lett.* **2006**, *88*, 073508.
(23) Park, S. H.; Roy, A.; Beaupré, S.; Cho, S.; Coates, N.; Moon, J. S.; Moses, D.; Leclerc, M.; Lee, K.; Heeger, A. J. Bulk Heterojunction Solar Cells with Internal Quantum Efficiency Approaching 100%. *Nat. Photonics.* **2009**, *3*, 297−303.
(24) Chen, L.; Xie, C.; Chen, Y. Influences of Charge of Conjugated Polymer Electrolytes Cathode Interlayer for Bulk Heterojunction Polymer Solar Cells. *Org. Electron.* **2013**, *14*, 1551−1561.
(25) Zhou, Y.; Fuentes-Hernandez, C.; Shim, J.; Meyer, J.; Giordano, A.; Li, H.; Winget, P.; Papadopoulos, T.; Cheun, H.; Kim, J.; Fenoll, M.; Dindar, A.; Haske, W.; Najafabadi, E.; Khan, T. M.; Sojoudi, H.; Barlow, S.; Graham, S.; Brédas, J.-L.; Marder, S.; Kahn, A.; Kippelen, B. A Universal Method to Produce Low-Work Function Electrodes for Organic Electronics. *Science* **2012**, *336*, 327−336.
(26) Park, Y.; Choong, V.; Gao, Y.; Hsieh, B.; Tang, C. Work Function of Indium Tin Oxide Transparent Conductor Measured by Photoelectron Spectroscopy. *Appl. Phys. Lett.* **1996**, *68*, 2699−2710.
(27) Scharber, M. C.; Mühlbacher, D.; Koppe, M.; Denk, P.; Waldauf, C.; Heeger, A. J.; Brabec, C. J. Design Rules for Donors in Bulk-Heterojunction Solar Cells-Towards 10% Energy Conversion Efficiency. *Adv. Mater.* **2006**, *18*, 789−794.
(28) He, Y.; Chen, H.; Hou, J.; Li, Y. Indene-C60 Bisadduct: A New Acceptor for High Performance Polymer Solar Cells. *J. Am. Chem. Soc.* **2010**, *132*, 1377−1382.
(29) Xia, R.; Leem, D.; Kircharts, T.; Spencer, S.; Murphy, C.; He, Z.; Wu, H.; Su, S.; Cao, Y.; Kim, J.; deMello, J.; Bradley, D.; Nelson, J. Investigation of a Conjugated Polyelectrolyte Interlayer for Inverted Polymer:Fullerene Solar Cells. *Adv. Energy Mater.* **2013**, *3*, 718−723.
(30) He, Z.; Zhong, C.; Huang, X.; Wong, W.; Wu, H.; Chen, L.; Su, S.; Cao, Y. Simultaneous Enhancement of Open-Circuit Voltage, Short-Circuit Current Density, and Fill Factor in Polymer Solar Cells. *Adv. Mater.* **2011**, *23*, 4636−4643.
(31) Lee, J.; Kang, H.; Kong, J.; Lee, K. A Depletion-Free, Ionic, Self-Assembled Recombination Layer for Tandem Polymer Solar Cells. *Adv. Energy Mater.* **2014**, DOI: 10.1002/aenm.201301226.
(32) Bilby, D.; Amonoo, J.; Sykes, M.; Frieberg, B.; Huang, B.; Hungerford, J.; Shtein, M.; Green, P.; Kim, J. Reduction of Open Circuit Voltage Loss in a Polymer Photovoltaic Cell via Interfacial Molecular Design: Insertion of a Molecular Spacer. *Appl. Phys. Lett.* **2013**, *103*, 203902.
(33) Liu, J.; Shao, S.; Fang, G.; Meng, B.; Xie, Z.; Wang, L. High-Efficiency Inverted Polymer Solar Cells with Transparent and Work-Function Tunable MoO_3-Al Composite Film as Cathode Buffer Layer. *Adv. Mater.* **2012**, *24*, 2774−2770.
(34) Braun, S.; Salaneck, W.; Fahlman, M. Energy-Level Alignment at Organic/Metal and Organic/Organic Interfaces. *Adv. Mater.* **2009**, *21*, 1450−1472.
(35) Kim, J.; Guan, Z.; Shu, A.; Kahn, A.; Loo, Y. Annealing Sequence Dependent Open-Circuit Voltage of Inverted Polymer Solar Cells Attributable to Interfacial Chemical Reaction between Top Electrodes and Photoactive Layers. *Langmuir* **2011**, *27*, 11265−11271.
(36) Yang, J.; Schumann, S.; Hatton, R.; Jones, T. Copper Hexadecafluorophthalocyanine (F16CuPc) as an Electron Accepting Material in Bilayer Small Molecule Organic Photovoltaic Cells. *Org. Electron.* **2010**, *11*, 1399−1402.
(37) Wang, N.; Yu, J.; Lin, H.; Jiang, Y. Organic Photovoltaic Cells with Improved Performance Using Bathophenanthroline as a Buffer Layer. *Chin. J. Chem. Phys.* **2010**, *23*, 84−88.
(38) Mutolo, K.; Mayo, E.; Rand, B.; Forrest, S.; Thompson, M. Enhanced Open-Circuit Voltage in Subphthalocyanine/C60 Organic Photovoltaic Cells. *J. Am. Chem. Soc.* **2008**, *128*, 8108−8109.
(39) Tress, W.; Leo, K.; Riede, M. Influence of Hole-Transport Layers and Donor Materials on Open-Circuit Voltage and Shape of I−V Curves of Organic Solar Cells. *Adv. Funct. Mater.* **2011**, *21*, 2140−2149.
(40) Tress, W.; Inganas, O. Simple Experimental Test to Distinguish Extraction and Injection Barriers at the Electrodes of (Organic) Solar Cells with S-Shaped Current−Voltage Characteristics. *Sol. Energy Mater. Sol. Cells* **2013**, *117*, 599−603.
(41) Sugiyama, K.; Ishii, H.; Ouchi, Y.; Seki, K. Dependence of Induim-Tin-Oxide Work Function on Surface Cleaning Method as Studied by Ultraviolet and X-Ray Photoemission Spectroscopies. *J. Appl. Phys.* **2000**, *87*, 295−298.
(42) Zhang, F.; Ceder, M.; Inganas, O. Enhancing the Photovoltage of Polymer Solar Cells by Using a Modified Cathode. *Adv. Mater.* **2007**, *19*, 1835−1838.
(43) Chen, F.; Chien, S. Nanoscale Functional Interlayers Formed Through Spontaneous Vertical Phase Separation in Polymer Photovoltaic Devices. *J. Mater. Chem.* **2009**, *19*, 6865−6869.
(44) Wang, H.; Zhang, W.; Xu, C.; Bi, X.; Chen, B.; Yang, S. Efficiency Enhancement of Polymer Solar Cells by Applying Poly(vinylpyrrolidone) as a Cathode Buffer Layer via Spin Coating or Self-Assembly ACS. *Appl. Mater. Interfaces* **2012**, *5*, 26−34.
(45) Baibarac, M.; Baltog, I.; Lefrant, S.; Mevellec, J.; Bucur, C. Vibrational and Photoluminescence Properties of the Polystyrene Functionalized Single-Walled Carbon Nanotubes. *Diamond Relat. Mater.* **2008**, *17*, 1380−1388.
(46) Moon, J.; Jo, J.; Heeger, A. Nanomorphology of PCDTBT:PC70BM Bulk Heterojunction Solar Cells. *Adv. Energy Mater.* **2012**, *2*, 304−308.

(47) Sachs-Quintana, I.; Heumuller, T.; Mateker, W.; Orozco, D.; Cheacharoen, R.; Sweetnam, S.; Brabec, C.; McGehee, M. Electron Barrier Formation at the Organic-Back Contact Interface is the First Step in Thermal Degredation of Polymer Solar Cells. *Adv. Funct. Mater.* **2014**, DOI: 10.1002/adfm.201304166.
(48) Xu, Z.; Chen, L.; Yang, G.; Huang, C.; Hou, J.; Wu, Y.; Hsu, C.; Yang, Y. Vertical Phase Separation in Poly(3-hexylthiophene): Fullerene Derivative Blends and its Advantage for Inverted Structure Solar Cells. *Adv. Funct. Mater.* **2009**, *19*, 1227−1234.
(49) Tremolet de Villers, B.; Tassone, J.; Tolbert, S.; Schwartz, B. Improving the Reproducibility of P3HT:PCBM Solar Cells by Controlling the PCBM/Cathode Interface. *J. Phys. Chem. C* **2009**, *113*, 18978−18982.